패널존 강도 및 보 웨브 접합방식이 RBS 철골 모멘트접합부의 내진거동에 미치는 영향

Cyclic Seismic Performance of Reduced Beam Section Steel Moment Connections: Effects of Panel Zone Strength and Beam Web Connection

이철호* 전상우** 김진호**
Lee, Cheol Ho Jeon, Sang Woo Kim, Jin Ho

국문요약

본 연구는 8개의 RBS (reduced beam section) 내진 철골모멘트접합부의 실물대 실험결과를 요약한 것이다. 본 실험의 주요변수는 보 웨브 접합법 및 패널존 강도를 택하였다. 균형 패널존 시험체는 접합부의 내진성능을 감소시키지 않으면서, 보와 패널존이 함께 균형적으로 지진에너지를 소산시키도록 설계하여 값비싼 패널존보강판(doubler plates)의 수요를 줄이고자 시도한 것이다. 보 웨브를 용접한 시험체는 모두 특별 연성모멘트골조에서 요구되는 접합부 회전능력을 충분히 발휘하였다. 반면 보 웨브를 볼트접합한 시험체는 조기에 스캘럽을 가로지르는 취성파단이 발생하는 열등한 성능을 보였다. 보 그루브 용접부 자체의 취성파괴가 본 연구에서와 같이 양질의 용접에 의해 방지되면, 스켈럽 부근의 취성파단이 다음에 해결해야 할 문제로 대두되는 경향을 보인다. 보 웨브를 볼팅한 경우에 접합부 취성파단의 빈도가 월등히 높은 이유를 실험 및 해석결과를 토대로 제시하였다. 측정된 변형도 데이터에 의할 때, 접합부의 전단력 전달메카니즘은 흔히 가정하는 고전 휨이론에 의한 예측과 전혀 다르다. 이는 전통적 보 웨브 설계법을 재검토할 필요가 있음을 시사하는 것이다. 아울러, 본 연구의 제한된 실험자료 및 접합부에서 요구되는 바람직한 거동기준을 근거로 균형 패널존의 강도범위에 대한 예비적 추정치를 제시하였다.

1. INTRODUCTION

As a response to the widespread damage in connections of steel moment-resisting frames that occurred during the 1994 Northridge, California and the 1995 Kobe, Japan earthquakes, a number of improved beam-to-column connection design strategies have been proposed. Of a variety of new designs, the reduced beam section (RBS) connection has exhibited satisfactory levels of ductility in numerous tests and has found broad acceptance in a relatively short time (Chen 1996; Plumier 1997; Zekioglu et al. 1997; Engelhardt et al. 1998). In the RBS connection a portion of the beam flange at some distance from the column face is strategically removed to promote stable yielding at the reduced section and to effectively protect the more vulnerable welded joints. This weakening strategy also reduces the seismic force demand on

* Assoc. Professor, Dept. of Architecture, Seoul National University
** Research engineer, Research Institute of Industrial Science and Technology

the column and the panel zone. Although this type of moment connections has been widely used in the past few years, there remain several design issues that should be further examined (for example, Jones et al. 2002; Gilton and Uang 2002; Chi and Uang 2002). The primary objective of this experimental study was to investigate the effects of the beam web connection and panel zone strength on seismic performance of the RBS connection.

2. TESTING PROGRAM

2.1 Design of Test Specimens

A total of eight full-scale test specimens were designed and classified as Set #1 and Set #2 (Table 1). Typical geometry and seimsic moment profile for the design of the radius-cut RBS are shown in Figs. 1 and 2. RBS was designed by referring to the recommendations by Iwankiw (1997) and Engelhardt et al. (1998). The beam end length (a) and the total length of the RBS zone (b) were chosen as 25% and 75% of the beam depth, respectively. These dimensions were selected to minimize the reduction in flange area. The resulting RBS eccentricity from the column face was 62.5% of the beam depth. The strain hardened plastic moment at the RBS hinge was calculated using the expected yield stress of the beam (F_{ye}= 313 MPa) and a strain hardening factor of 1.1.

$$m_p^{act} = \alpha \times Z_{RBS} \times F_{ye} = (1.1) \times Z_{RBS} \times F_{ye} \tag{1}$$

The trimmed flanges were then sized to limit the moment at the column face to the expected elastic limit moment of the whole beam section as follows.

$$S \times F_{ye} \geq M_f = m_p^{act} \times \left(\frac{L_b}{L} \right) \tag{2}$$

where S = elastic section modulus of the beam.

The reduction in flange area at the RBS center was 37% and 40% for Set #1 and Set #2, respectively (see Table 1). The flange reduction in Set #1 was slightly less than the 40% minimum reduction limit of the SAC recommendation (SAC 2000).

The panel zones were then designed either of the following two equations for the panel zone strength:

$$V_{pz} = (0.75)(0.6 F_{yc} d_c t_p) \left[1 + \frac{3 b_{cf} t_{cf}^2}{d_b d_c t_p} \right] \tag{3}$$

$$V_{pz} = (1.0)(0.6 F_{yc} d_c t_p) \left[1 + \frac{3 b_{cf} t_{cf}^2}{d_b d_c t_p} \right] \tag{4}$$

where F_{yc}=the yield stress of the column web, d_b=the beam depth, d_c= the column depth, t_p=the thickness of the panel zone, b_{cf}= the column flange width, and t_{cf}= the column flange thickness. Eq. (3) is implemented in the AISC seismic provision (AISC 1997). Specimens satisfying the requirement in Eq. (3) were classified as strong panel zone specimens. In Set #1, nominally identical steel shapes were used. When Eq. (3) was used for the panel zone strength, doubler plates of 10 mm thickness were provided to specimens DB700-SB and DB700-SW. The doubler plates were plug-welded to the column web to prevent premature local buckling under large cyclic inelastic shear deformations (AISC 1997, AWS D1.1 2000). Beam-like deep column was employed to obtain strong panel zone specimens in Set #2 (specimens DEEP-80 and DEEP-90). To prevent possible column twisting associated with the

deep-column RBS connections, the combined stress level at the column flange was limited to 80% and 90% of the column yield stress by following the design verification procedure proposed by Chi and Uang (2002); no column twist was observed from these specimens during the test. Based on Krawinkler's recommendation (Krawinkler 1978), the medium panel zone specimens were designed using Eq. (4); in essence the resistance factor of 0.75 in Eq. (3) was simply set to 1.0 to promote some limited panel zone yielding. Four medium panel zone specimens in total were prepared in this testing program (DB700-MB and DB700-MW in Set #1, DB600-b85 and DB600-b65 in Set #2). Two specimens DB600-b85 and DB600-b65 in Set #2 were identical except a slight difference in RBS length, that is, the RBS length was taken as 85% (DB600-b85) and 65% (DB600-b65) of the beam depth.

Most of past tests have been conducted on specimens with a fully welded beam web. Two bolted web specimens, DB700-SB and DB700-MB, were included in Set #1 to compare directly the effects of different beam web connection methods. With a slip coefficient of 0.33, the slip-critically designed bolted web connection consisted of eight-M22-F10T fully tensioned bolts. The bolts were tightened with the calibrated wrench method up to the specified tension level of 201 (kN). The ultimate strength of bolted web connection was about two times the expected maximum beam shear. In Set #2, all the beam webs were groove-welded to the column flange.

In specimens DB600-b85 and DEEP 80, ceramic backup bars were used in order to make notch-free groove welded joint more economically; removing ceramic backup bars was much easier than steel backup bars and simple cosmetic fillet weld was added. Specimens with ceramic back bars performed satisfactorily as well. The continuity plates equal in thickness to the beam flange were provided in all specimens. Welding electrodes with a specified minimum CVN toughness of 26.7 Joule at -28.9°C (20 ft-lb at -20°F) was used. Weld access hole configurations followed the SAC recommendations (SAC 2000). Fig. 3 and 4 show the connection details for specimens DB700-SW and DB700-SB. In specimen designation of Set #1, following abbreviations were used: S= strong panel zone, M= medium panel zone, W= welded web, and B= bolted web. Steel coupons were cut from the beam and column shapes after the test. Tensile coupon test results are summarized in Table 2.

2.2 Test Setup and Loading

The specimens were mounted to a strong floor and a strong wall. An overall view of typical test setup is shown in Fig. 5. A servo-controlled actuator, capable of applying loads up to 1961 kN and displacements of up to ±300 mm was used. Lateral restraint was provided at a distance of 2500 mm from the column face. The specimens were tested statically according to SAC standard loading protocol (SAC 2000) as shown in Fig. 6. The beam tip displacement corresponding to the story drift ratio of 1% was 38 (mm). The test specimens were instrumented with a combination of displacement transducers and strain gages to measure global and local responses. Whitewash was painted around the connection to monitor yielding during the test.

3. TEST RESULTS AND DISCUSSIONS

The cyclic responses from Set #1 in terms of the story drift ratio are presented in Fig. 7. The ordinate is expressed in terms of the normalized moment at the column face. The

normalization was based on the nominal plastic moment of the original (unreduced) beam section. Both strong and medium panel zone specimens with a welded web connection developed satisfactory levels of ductility required of special moment frames. On the other hand, specimens with a bolted web connection performed poorly due to premature brittle fracture of the beam flange at the weld access hole (see Figs. 8 and 9). Specimens DB700-SB and DB700-MB failed in a brittle manner at the 2% and 3% story drift cycle, respectively. A complete fracture across the beam flange width was developed. Figs. 10 and 11 show the plastic hinge formation in specimens with a welded web connection. Significant yielding of the panel zone in specimen DB700-MW was evidenced by the flaking of the whitewash. Specimen DB700-SW exhibited excellent connection rotation capacity up to 6% story drift without fracture. Fig. 12 shows comparison of the normalized maximum moment transferred to the column. The normalization was based on the actual plastic moment of the original (unreduced) beam section. It is observed from Fig. 12 that, unlike the case of the welded web specimens, the bolted web specimens were not able to transfer the actual plastic moment of the whole beam section to the column.

Simple "demand to capacity" study was conducted to investigate the base metal fracture of specimen DB700-SB from the engineering mechanics perspective. Considering that the mode of failure was premature brittle fracture type, simple elastic analysis was still considered useful. The solid elements in the general purpose finite element analysis program SAP 2000 (CSI 1997) were used to analyze the three-dimensional test subassembly. An observed fracture load of 510 kN was applied to the beam tip to obtain the flexural and shear stress distributions around the weld access hole. Two idealized cases were considered in the analysis: (a) the bolted beam web was not able to transfer moment and shear, and (b) the bolted beam web is fully active as all-welded connection. Fig. 13 shows the stress distributions from the finite element analysis results. High stress concentration at the weld access hole was evident in both cases. The maximum flexural stress level predicted by the beam theory was 318 MPa. The maximum tensile principal stresses from the finite element analyses of the two cases were 554 MPa and 460 MPa, respectively, for both cases, which exceed the measured tensile strength of the beam flange (455 MPa, see Table 2). Tsai and Popov (1988) indicated that web bolts typically slip during testing, leaving the stiffer welded flange alone to resist the total applied moment. If it is speculated that the actual situation in bolted web connections falls somewhere between two idealized cases, simple "maximum tensile strength fracture criterion" seems to be sufficient to explain a higher incidence of base metal fracture in specimens with bolted web connections. Fig. 14 compares the cyclic flexural strain responses near the groove weld up to the fracture point of specimen DB700-SB. Much higher strain demand on the bolted web specimen is evident.

According to Dexter and Melendrez (2000), the tensile capacity of a welded joint made with a filler metal having a specified minimum CVN toughness of 26.7 Joule at -28.9°C (20 ft-lb at -20°F) is significantly higher than the tensile strength of weld metal because of the tri-axial stress constraint. It is noteworthy that no fracture occurred within the groove welds of any connection of the eight specimens. Considering all these, the area more susceptible to fracture may be located near the line B-B' or C-C', rather than the line A-A'. Moreover, the steel material in this area is heat-affected due to welding and thermal cutting of weld access hole. It is noted that, among the six web welded specimens, two specimens (DB700-MW and DEEP 90) eventually failed in a brittle manner at the weld access hole during the first positive

excursion of the 5% story drift cycle. It appears that the failure is related to both low-cycle fatigue and stress concentration at the weld access hole.

By assuming that the beam web is fully active (Fig. 13b), shear transfer by one beam flange through the line A-A' or B-B' is still as high as 30% of the total. Goel et al. 1997 pointed out that the area in the middle of the beam web near the shear tab is virtually devoid of stresses and much of the shear force is transferred through the beam flanges, thus leading to overstressing the beam flanges. Plastic straining of the beam flange leads to a redistribution of shear stress. However, very large plastic strain in the beam flanges, or such strains that must be avoided, would be needed for the shear force distribution to approach that of the beam theory (Kim, et al. 2002). Measured cyclic shear strain responses are presented in Figs. 15 and 16. These measured results evidence the foregoing observations. Reverse shear occurs in the middle of the beam web. This is undesirable because reverse shear will increase shear demand on the other part of the connection to meet the force equilibrium. The shear transfer mechanism in the RBS connection is still not consistent with that predicted by the classical beam theory and should be reexamined more thoroughly. In this context, the practice of providing web bolts uniformly along the beam depth needs to be reconsidered.

The plots shown in Fig. 17 indicate that all specimens in Set #2, with both strong and medium panel strength, exhibited satisfactory connection ductility required of special moment frames. Fig. 18 shows a comparison of the connection strength between the medium and strong panel zone specimens in terms of the normalized maximum moment transferred to the column. It is observed that the medium panel zone specimens also transferred the actual plastic moment of the whole beam section to the column. Fig. 19 presents the comparison of lateral torsional buckling (LTB) amplitudes measured up to the 4% story drift cycle. As expected, due to sharing of plastic rotation between the panel zone and the beam in the medium panel zone specimens, LTB amplitudes were reduced. This is a sure advantage to reducing the increased tendency of global instability of the beam having RBS connections. The strain hardening factor, computed at the RBS center based on the measured tensile properties, was of similar magnitude between the medium and strong panel zone specimens, and reached an average value of 1.27 at the 4% story drift cycle in this testing program. (see Fig. 20). This value is higher that usually assumed (1.1~1.15) in design (AISC 1997).

The effects of panel zone strength on some connection responses are summarized in Table 3. For the purpose of analyzing the effects of panel zone strength, two formulae were used as a measure of the panel zone strength in this study; one is based on the Von Mises yield criterion (Eq. 5), and the other is based on Krawinkler's recommendation which includes the contribution of column flange to the post-yield strength (Eq. 6). The measured yield strength in Table 2 was used to calculate the panel zone strength.

$$V_y = 0.577 F_{yc} d_c t_p \approx 0.6 F_{yc} d_c t_p \tag{5}$$

$$V_p = (0.6 F_{yc} d_c t_p)\left[1 + \frac{3 b_{cf} t_{cf}^2}{d_b d_c t_p}\right] \tag{6}$$

As a measure of the beam strength, the panel zone shear force $V_{RBS,P}$ corresponding to the actual plastic moment of the RBS was used; a similar strength measure was used by Roeder (2002). For a one-sided moment connection, $V_{RBS,P}$ can be computed as follows:

$$V_{RBS,P} = \left(\frac{M_{RBS,P}}{d_b}\right) \times \left(\frac{L_b/2 + d_c/2}{L_b/2 - e}\right) \times \left(1 - \frac{d_b}{H_c}\right) \tag{7}$$

where $M_{RBS,P}$ = actual plastic moment at the RBS based on the measured yield stress, d_b = beam depth, d_c = column depth, H_c = column height, and refer to Fig. 2 for the remaining symbols. With a panel zone strength ratio of $V_y/V_{RBS,P}$=0.93 (specimen DB700-MW), Fig. 21 shows an example of the cumulative energy dissipation and the panel zone shear response; the panel zone dissipated about 40% of the total energy and developed about 1% radian plastic rotation up to the 4% story drift cycle. Unfortunately, the tensile coupon test results for the doubler plates in specimen DB700-SW were not available and this specimen was omitted in Table 3. To augment the database, one test result by Chi and Uang (2002) was included. It is observed from Table 3 that, within rather broad ranges of the relative panel zone strength, the panel zone provided about 0.01 rad. plastic rotation and dissipated 30%~40% of the total energy. Based on these limited test data, preliminary estimates of the balanced panel zone strength may be proposed as follows.

$$0.9 \le \frac{V_y}{V_{RBS,P}} \le 1.2 \tag{8}$$

or,

$$1.1 \le \frac{V_p}{V_{RBS,P}} \le 1.4 \tag{9}$$

The range recommended above was an attempt to achieve the following: (i) reduced fabrication cost, (ii) the panel zone to provide about 0.01 rad. plastic rotation out of the total plastic rotation of 0.03 rad., (iii) the panel zone to dissipate 30%~40% of the total energy up to the 4% story drift cycle under the "standard" cyclic loading, (v) reduced LTB amplitude for less distortion of the beam.

4. SUMMARY AND CONCLUSIONS

The results of this study are summarized as follows.

(1) Both strong and medium panel zone specimens with welded web connection exhibited satisfactory levels of connection ductility required of special moment frames. Specimens with a less costly bolted web connection performed poorly due to premature brittle fracture of the beam flange at the weld access hole. Unlike web-welded specimens, specimens with a bolted web connection could not transfer actual plastic moment of the whole beam section to the column. Further reduction of the beam flanges for the bolted web connections may be justified with due consideration of the measured connection strength and strain hardening factor.

(2) If fracture within the beam flange groove weld was avoided using quality welding, fracture tended to move into the beam flange base metal at the weld access hole. Based on the experimental and analytical results, the observed base metal fracture at the weld access hole was explained from the engineering mechanics perspective. The measured strain data confirmed that the classical beam theory dose not provide a reliable shear transfer prediction. The results of this study also suggest that the practice of providing web bolts uniformly along the beam depth needs to be reconsidered.

(3) Criteria for a balanced PZ strength that improves the plastic rotation capacity while reduces the amount of beam distortion are proposed.

REFERENCES

1. Chen, S. J., Yeh, C. H., and Chu, J. M. (1996). "Ductile steel beam-to-column connections for seismic resistance." J. Struct. Engrg., ASCE, 122(11), 1292-1299.
2. Chi, B. and Uang, C.-M. (2002). "Cyclic Response and Design Recommendations of Reduced Beam Section Moment Connections with Deep Column." J. Struct. Engrg., ASCE, 128(4), 464-473.
3. Dexter, R. J. and Melendrez, M. I. (2000). "Through-thickness Properties of Column Flanges in Welded Moment Connections." J. Struct. Engrg., ASCE, 126(1), 24-31.
4. Engelhardt, M. D., Winneberger, T., Zekany, A. J., Potyraj, T. J., (1998). "Experimental Investigations of Dogbone Moment Connections." Engrg. J., 35(4), AISC, Fourth Quarter, 128-139
5. Gilton, C. S. and Uang, C.-M. (2002). "Cyclic Response and Design Recommendations of Weak-Axis Reduced Beam Section Moment Connections." J. Struct. Engrg., ASCE, 128(4), 452-463
6. Goel, S. C., Stojadinovic, B., and Lee, H.-K. (1997). "Truss analogy for steel moment connections", Eng. J. 34(2), 43-53.
7. Iwankiw, N. (1997). "Ultimate Strength Consideration for Seismic Design of the Reduced Beam Section (Internal Plastic Hinge)." Engrg. J., AISC, 34(1), First Quarter, 3-16.
8. Jones, S. L., Fry, G. T., and Engelhardt, M. D. (2002). "Experimental Evaluation of Cyclically Loaded Reduced Beam Section Moment Connections." J. Struct. Engrg., ASCE, 128(4), 441-451.
9. Kim, T., Whittaker, A. S., Gilani, A. S. J., Bertero, V. V., and Takhirov, S. M. (2002), "Cover-Plate and Flange-Plate Steel Moment-Resisting Connections." J. Struct. Engrg., ASCE, 128(4), 474-482.
10. Krawinkler, H. (1978). "Shear in Beam-Column Joints in Seismic Design of Steel Frames." Engrg. J., AISC, 15(3), Third Quarter, 82-91
11. Plumier, A. (1997). "The Dogbone: Back to the Future." Engrg. J., AISC, 34(2), Second Quarter, 61-67
12. Roeder, C. W. (2002). "General Issues Influencing Connection Performance." J. Struct. Engrg., ASCE, 128(4), 420-428.
13. SAC (2000). "Seismic Design Criteria for New Moment-Resisting Steel Frame Construction." Report No. FEMA 350, SAC Joint Venture, Sacramento, CA.
14. SAP 2000 (1998). Analysis Reference Vol. I and II, Computer and Structures, INC., Berkeley, CA.
15. Seismic Provisions for Structural Steel Buildings. (1997). 2nd Ed., AISC, Chicago, IL.
16. Structural Welding Code-Steel (2000). AWS D1.1: Section 3.10, American Welding Society,
17. Tsai, K. C. and Popov, E. P. (1988) "Steel Beam-Column Joints in Seismic Moment Resisting Frames." EERC Report, UCB/EERC-88/19, Univ. of Calif., Berkeley.
18. Zekioglu, A., Mozaffarian, H., Chang, K. L., and Uang, C.-M.(1997). "Designing after Northridge." Modern Steel Constr., 37 (3), 36-42.

Table 1. Test Specimen

Specimen	Beam and column	Panel zone Strength	Beam web connection method	a (㎜)	b (㎜)	c (㎜)	Flange reduction (%)
			Set #1				
DB700-SW	H700X300X13X24 (SS400) H428X407X20X35 (SM490)	Strong(10㎜doubler plate, SM490)	Welded	175	525	55	37
DB700-MW	H700X300X13X24 (SS400) H428X407X20X35 (SM490)	Medium	Welded	175	525	55	37
DB700-SB	H700X300X13X24 (SS400) H428X407X20X35 (SM490)	Strong(10㎜ doubler plate, SM490)	Bolted	175	525	55	37
DB700-MB	H700X300X13X24 (SS400) H428X407X20X35 (SM490)	Medium	Bolted	175	525	55	37
			Set #2				
DB600-b85 (ce)*	H600X200X11X17 (SS400) H400X400X13X21 (SM490)	Medium	Welded	150	510	40	40
DB-600-b65	H600X200X11X17 (SS400) H400X400X13X21 (SM490)	Medium	Welded	150	390	40	40
DEEP-80** (ce)*	H600X200X11X17 (SS400) H588X300X12X20 (SM490)	Strong	Welded	150	450	40	40
DEEP-90**	H606X201X12X20 (SS400) H588X300X12X20 (SM490)	Strong	Welded	150	450	40	40

* Ceramic backup bars were used,

** Deep column specimens,

Table 2. Tensile Coupon Test Results

Member	Coupon	Yield stress (MPa)	Tensile strength (MPa)	Elongation (%)***
Beam H700X300X13X24(SS400)	Flange	304	455	67
	Web	364	480	76
Column H428X407X20X35(SM490)	Flange	343	512	67
	Web	358	520	69
Beam H600X200X11X17(SS400)	Flange	326	467	70
	Web	343	473	73
Column H400X400X13X21(SM490)	Flange	358	525	68
	Web	374	531	74
Beam H606X201X12X20(SS400)	Flange	295	447	66
	Web	333	471	71
Column H588X300X12X20(SM490)	Flange	374	534	70
	Web	405	546	74

*** Based on the gage length of 200 mm.

Table 3. Effects of panel zone strength on plastic rotation and energy dissipation

Specimen	PZ strength relative to beam		Panel zone plastic rotation at 4% story drift ratio (rad)	Energy dissipation by panel zone up to 4% story drift cycle (%)
	$V_y/V_{RBS.P}$	$V_P/V_{RBS.P}$		
DB700-MW	0.93	1.15	0.012	43
DB600-b85	1.03	1.20	0.008	32
DB600-b65	1.05	1.22	0.009	30
DC2*	1.36	1.50	0.005	NA
DEEP-90	1.40	1.52	0.0002	5 %
DEEP-80	1.48	1.60	Negligible	Negligible

* Chi and Uang (2002)

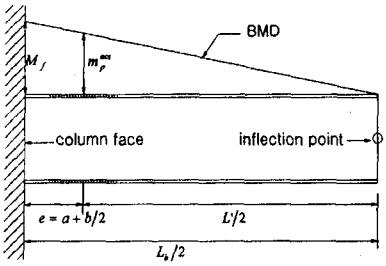

Fig. 1 Typical geometry of the radius cut RBS

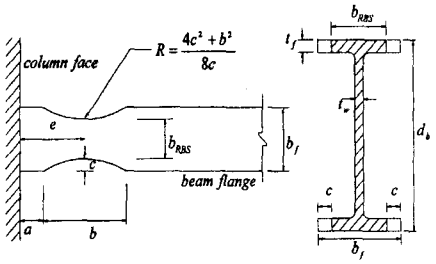

Fig. 2 Moment profile for RBS design

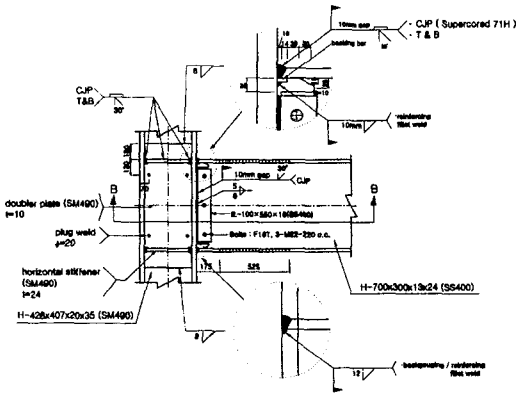

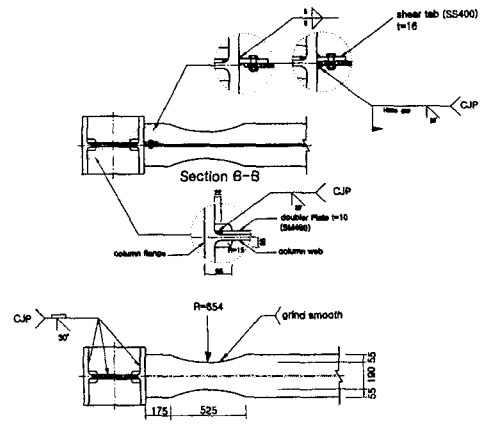

Fig. 3 Specimen DB700-SW moment connection details

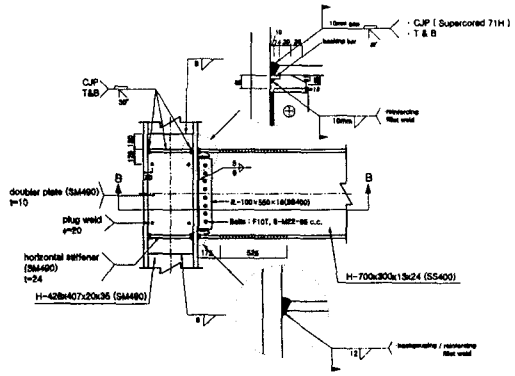

Fig. 4 Specimen DB700-SB moment connection details

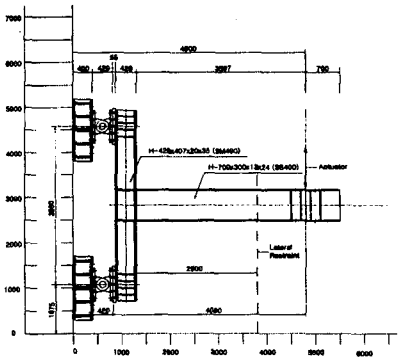

Fig. 5 Typical test setup

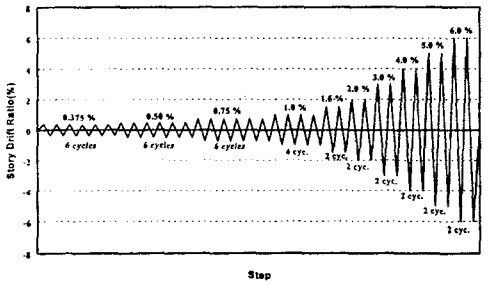

Fig 6 SAC 2000 standard loading history

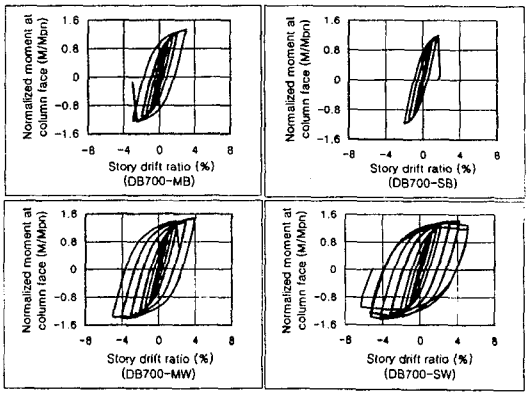

Fig. 7 Normalized moment versus story drift ratio relationship (test set #1)

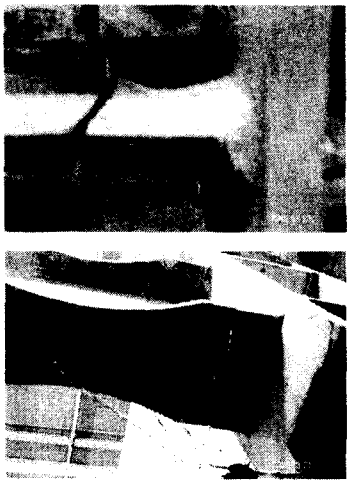

Fig. 8 Beam bottom flange fracture of specimen DB700-SB at 2% story drift cycle

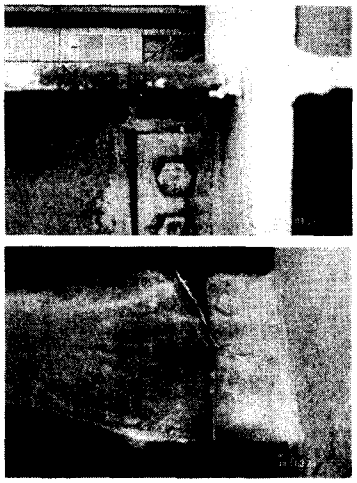

Fig. 9 Beam top flange fracture of specimen DB700-MB at 3% story drift cycle

Fig. 10 Connection region of specimen DB700-MW at 5% story drift cycle

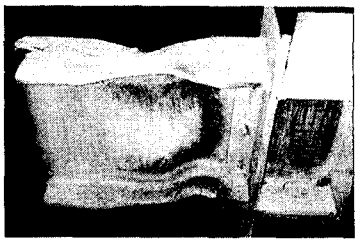

Fig. 11 Connection region of specimen DB700-SW at 6% story drift cycle

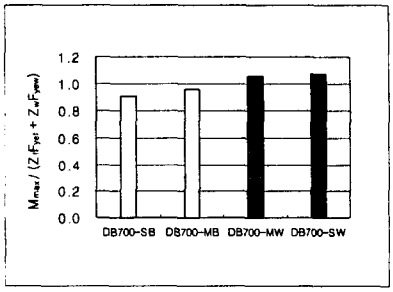

Fig. 12 Comparison of connection strength (set #1)

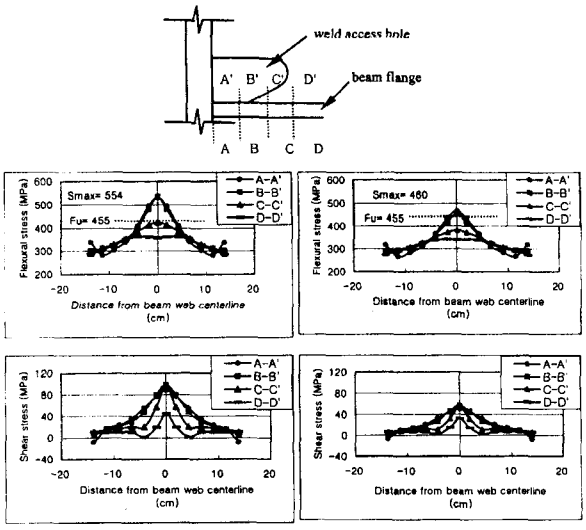

(a) (b)

Fig. 13 Analytical stress distribution around weld access hole at fracture load (specimen DB700-SB); (a) assuming that the beam web is totally inactive, (b) assuming that the beam web is fully active

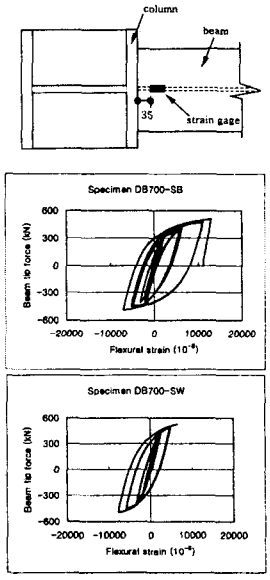

Fig. 14 Comparison of flexural strain responses near groove weld up to the fracture of specimen DB700-SB

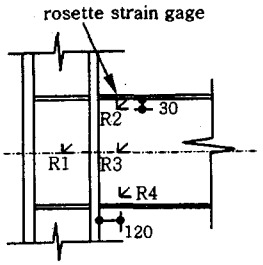

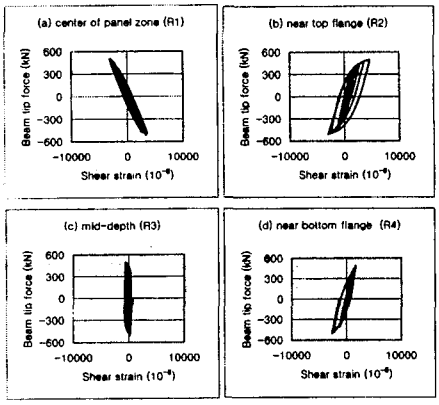

Fig. 15 Measured cyclic shear strain responses (specimen DB700-SB)

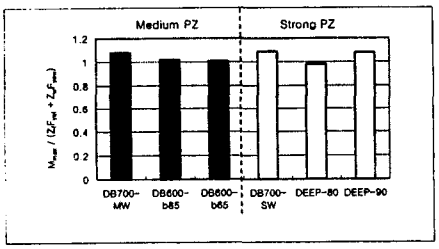

Fig. 18 Comparison of connection strength (medium versus strong panel zone)

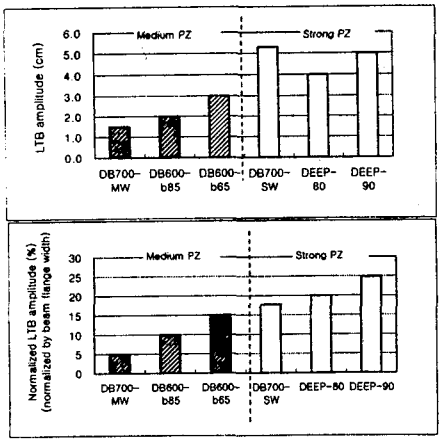

Fig. 19 Comparison of LTB amplitudes at the 2nd peak of 4% story drift

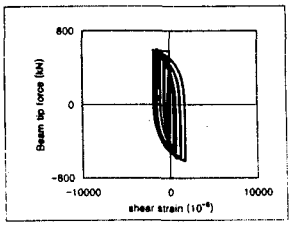

Fig. 16 Reverse shear measured at the rosette strain gage R3 (specimen DB700-MW)

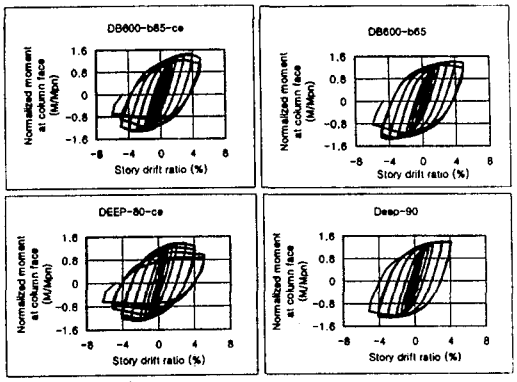

Fig. 17 Normalized moment versus story drift ratio relationship (test set #2)

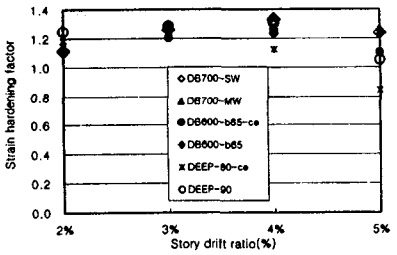

Fig. 20 Story drift ratio versus strain hardening factors

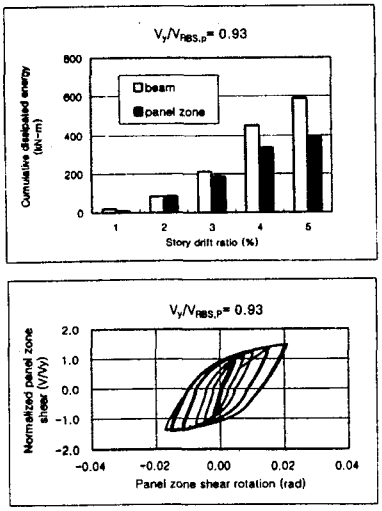

Fig. 21 Cumulative energy dissipation and cyclic shear response of the panel zone (DB700-MW)